JOURNAL OF AIRCRAFT
Vol. 35, No. 5, September–October 1998

Control-Surface Reversal in the Transonic Regime

G. Andersen* and R. Kolonay†
U.S. Air Force Research Laboratory, Wright–Patterson Air Force Base, Ohio 45433-7542
and
F. Eastep‡
University of Dayton, Dayton, Ohio 45469

A method of predicting control-surface reversal trends in the transonic flight regime is presented. Linear and nonlinear rigid and aeroelastic analyses are performed to examine the effects of including flow nonlinearities in the prediction of this aeroelastic phenomenon. Transonic small disturbance theory is employed in the analysis of a simple rectangular wing and a typical fighter-type wing to study the interactions among control-surface deflections, structural flexibility, and embedded shocks in the flowfield. Pressure distributions on the wings are examined. Rigid rolling moment calculations are presented, followed by control-surface effectiveness and control-surface reversal trends as the Mach number is varied from a subsonic value, through the transonic regime, into the supersonic region. Results indicate the importance of including aerodynamic nonlinearities in the steady aeroelastic analysis and design of lifting surfaces with deflected control surfaces subject to transonic flow conditions.

Nomenclature

C_M = rolling moment coefficient
C_{M_δ} = derivative of rolling moment coefficient with respect to control-surface deflection
C_p = pressure coefficient
c = root chord length
M = Mach number
q = dynamic pressure
x = chordwise location
γ = ratio of specific heats
ΔC_p = resultant pressure coefficient, $C_{p_l} - C_{p_u}$
ε = control-surface effectiveness

Subscripts
f = quantity is associated with an analysis that includes structural flexibility
l = quantity is associated with the lower surface of the wing
u = quantity is associated with the upper surface of the wing
r = quantity is associated with an analysis that does not include structural flexibility
∞ = freestream condition

Introduction

TO perform the structural design of flight vehicles, efficient and accurate maneuver load predictions are required. Currently, there are many well-established techniques available to determine steady aerodynamic loads and static aeroelastic responses in subsonic and supersonic flight. These methods are also currently used in the transonic region. Because these techniques are based on linear aerodynamic theory, they are efficient but not considered accurate in this regime. The transonic flow condition is a mixture of subsonic and supersonic flow with embedded shocks; therefore, to accurately describe the transonic flowfield, nonlinear partial differential equations must be solved.

Until recently, little effort has been expended to include nonlinear aerodynamic loads in the preliminary structural design environment because of the large computational cost associated with the solution of the nonlinear equations. With advances in nonlinear aerodynamic flow solvers and computer hardware, nonlinear airloads are now available at a reasonable computational cost. The intent of this research is to develop an efficient and accurate analysis that is capable of determining the steady aeroelastic response of a lifting surface with an articulated control surface in transonic flow. Of particular interest is the rolling performance of a lifting surface in transonic flow including aeroelastic effects. This study will investigate the impact of using nonlinear aerodynamics to determine the control-surface effectiveness values and reversal dynamic pressures as compared to those found using linear aerodynamics in the transonic flight regime.

Background

Aeroelastic analysis of flexible aircraft structures in the transonic flight regime is a relatively recent endeavor. In the late 1980s, research was conducted in the prediction of steady and unsteady airloads in the transonic region through the use of classical transonic small disturbance (TSD) theory,[1] and by employing the transonic full-potential equation.[2] Although both of these efforts included articulated control surfaces in the analysis, the effects of structural flexibility were not taken into account.

In 1991, TSD theory was utilized to predict dynamic and steady aeroelastic phenomena for the F-15 and F/A-18 aircraft.[3] Although rolling moment coefficients were not directly observed, the prediction of control-surface reversal dynamic pressure was offered at a single Mach number through examination of the behavior of the computed lift coefficient for a lifting surface.

Recently, there has been considerable interest in the U.S. Air Force in employing reduced stiffness wing structures to effect maneuver performance. A rigid analysis is not sufficient in cases where a flexible structure deforms under the generated

Presented as Paper 97-1385 at the AIAA/ASME/ASCE/AHS/ASC 38th Structures, Structural Dynamics, and Materials Conference, Kissimmee, FL, April 7–10, 1997; received June 16, 1997; revision received Feb. 5, 1998; accepted for publication April 27, 1998.

*Aerospace Engineer, Lieutenant U.S. Air Force, Air Vehicles Directorate, Structures Division.
†Aerospace Engineer, Air Vehicles Directorate, Structures Division. Member AIAA.
‡Professor, Department of Mechanical and Aerospace Engineering. Associate Fellow AIAA.

airloads. This issue was addressed under a U.S. Air Force contract with Rockwell International Corporation.[4] The study considered the effects of structural flexibility under the influence of airloads created by a deflected control surface. Degradation of rolling moment with increased dynamic pressure was shown for a limited range of Mach numbers. However, an in-depth investigation into the effect of varying Mach number and the interaction between shocks and control surfaces was not undertaken.

The present research effort focuses on a detailed examination of aeroelastic effects resulting from control-surface deflections in transonic flow. Emphasis is on the prediction of pressure distributions and steady aeroelastic phenomena including the effects of shocks located on the wing surface. Rolling moments and control-surface reversal points are examined as the Mach number is varied from subsonic to supersonic values.

Approach

Transonic Small Distrubance Theory

Because flow in the transonic region is affected by shocks, effective analyses in this regime must include these nonlinearities. The method employed in this study was TSD theory. Although one of the simplest forms of nonlinear aerodynamics, the TSD theory is capable of determining the strength and location of weak shocks and is generally considered adequate for preliminary design.

The aeroelastic calculations were performed by the NASA Langley code, CAP–TSD.[5] Using the finite difference method, the program solves the general frequency modified TSD potential equation, given here in differential form as

$$\frac{\partial f_0}{\partial t} + \frac{\partial f_1}{\partial x} + \frac{\partial f_2}{\partial y} + \frac{\partial f_3}{\partial z} = 0 \tag{1}$$

where

$$f_0 = -A\phi_t - B\phi_x, \qquad f_1 = E\phi_x + F\phi_x^2 + G\phi_y^2$$
$$f_2 = \phi_y + H\phi_x\phi_y, \qquad f_3 = \phi_z \tag{2}$$

The coefficients A, B, and E are defined as

$$A = M_\infty^2, \qquad B = 2M_\infty^2, \qquad E = 1 - M_\infty^2 \tag{3}$$

Within CAP–TSD there are a number of options for specifying the coefficients F, G, and H, depending upon the assumptions used in deriving the TSD equation. For the nonlinear analyses, the coefficients were

$$F = -\tfrac{1}{2}(\gamma + 1)M_\infty^2, \qquad G = -\tfrac{1}{2}(\gamma - 3)M_\infty^2, \qquad H = -M_\infty^2 \tag{4}$$

and for the linear cases

$$F \equiv G \equiv H \equiv 0 \tag{5}$$

Steady Aeroelastic Analysis

Aeroelastic analyses in CAP–TSD are performed in generalized modal coordinates. Required mode shapes were obtained through an eigenvalue analysis in which the structural stiffness and mass of the system were represented by the finite element method. Structural eigenvalues, eigenvectors, generalized mass, and generalized stiffness were determined using the automated structural optimization system (ASTROS).[6] The structural eigenvectors were then splined to the aerodynamic degrees of freedom, represented by the CAP–TSD mesh, using the infinite plate spline.[7] With the splined mode shapes and generalized mass and stiffness, the static aeroelastic analysis was performed using appropriate boundary conditions in CAP–TSD. This analysis yielded the velocity potentials and pressure coefficients at the mesh nodes. The CAP–TSD code was modified to include integration of the pressure coefficients to calculate a rolling moment.

Because steady-state roll performance was the subject of this study, a parameter used in the investigation of roll performance, control-surface effectiveness, was employed. Defined as the flexible to rigid ratio of the rolling moment stability derivative produced by a control-surface deflection at a given flight condition, control-surface effectiveness is given by the following equation:

$$\varepsilon = C_{M_{\delta,f}}/C_{M_{\delta,r}} \tag{6}$$

where the numerator and denominator are, respectively, the flexible and rigid derivatives of the rolling moment coefficients with respect to control-surface deflection. Assuming a constant angle of attack and control-surface deflection, the rigid rolling moment coefficient varies with Mach number only; however, this coefficient varies with Mach number and dynamic pressure as structural flexibility is included in the analysis.

The steady aeroelastic phenomenon of interest, control-surface reversal, occurs when ε passes through zero. The determination of control-surface effectiveness at various Mach numbers and dynamic pressures yields the control-surface reversal points. A plot of ε against dynamic pressure gives the reversal point for a particular Mach number. Doing this for a range of Mach numbers generates a curve indicating the behavior of the reversal dynamic pressure as the Mach number is varied. This procedure is carried out with both linear and nonlinear aerodynamic force calculations. Doing so allows the difference between the use of nonlinear and linear aerodynamics in the prediction of control-surface effectiveness and reversal points to be quantified.

Analysis Models

This analysis procedure was carried out on two independent wing models. The first, a rectangular wing, was originally used to demonstrate transonic flutter predictions,[8] and was modified for steady aeroelastic analyses. The structure is a beam model consisting of eight equal-length beam elements spanning the wing. The torsional stiffness and bending stiffness of the wing are 2.39×10^6 lbf ft^2 and 23.66×10^6 lbf ft^2, respectively. The beam axis was positioned such that the elastic axis was at the 1/3-chord location. Wing thickness was modeled with a 4% thick parabolic airfoil. A single trailing-edge control surfce was added for this study and spanned the outboard half of the wing. The applied small disturbance mesh consisted of a $60 \times 41 \times 30$ grid on a rectangular coordinate system with the x axis oriented streamwise and the y axis oriented out the span of the wing. The aerodynamic planform contained 39 chordwise and 33 spanwise grid points. The planform geometry and computational mesh of this wing are shown in Fig. 1.

The second wing model investigated was that of a generic fighter-type aircraft.[9] The structural model of the wing was a fully built-up finite element model with a stiffness representative of stiff, low-aspect-ratio fighter wings. A NACA 0004 airfoil represented the wing thickness. A single inboard trailing-edge control surface or flaperon was utilized. The full computational mesh for this model was a $96 \times 50 \times 70$ grid. Forty-six chordwise and 34 spanwise grid points were used on

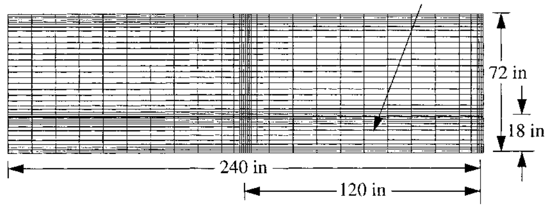

Fig. 1 Aerodynamic planform and CAP–TSD computational mesh for rectangular wing analyses.

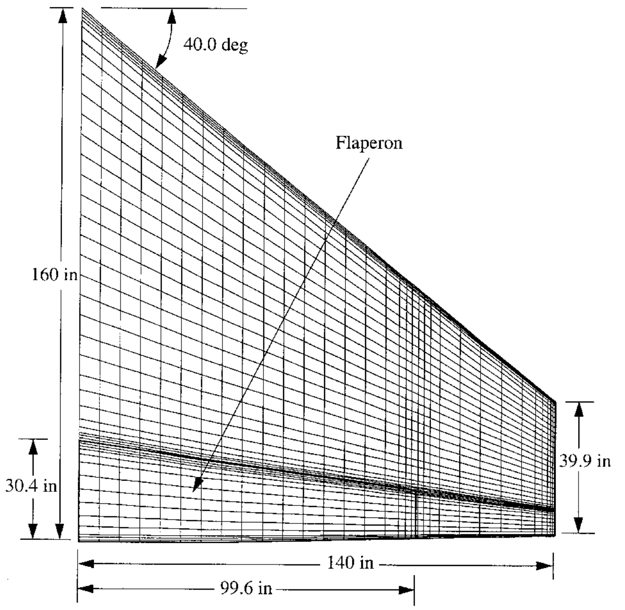

Fig. 2 Aerodynamic planform and CAP–TSD computational mesh for fighter wing analyses.

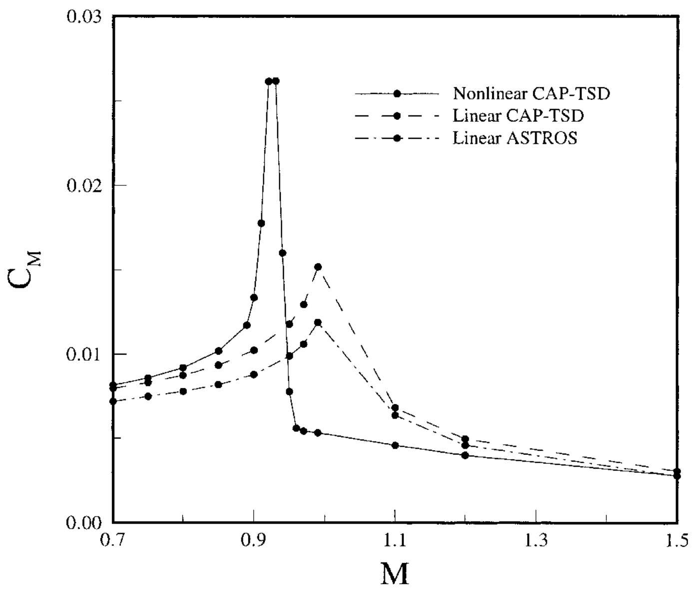

Fig. 3 Variation of rigid rolling moment coefficient with Mach number of rectangular wing.

the aerodynamic surface. The planform geometry and computational mesh of this wing are depicted in Fig. 2.

Rigid and flexible aeroelastic analyses were performed to obtain control-surface effectiveness values using both nonlinear and linear aerodynamics. Additional linear analyses were performed in ASTROS for the rectangular wing. Boundary conditions for both wings were identical and consisted of a cantilevered wing root, 0-deg initial angle of attack, and 1-deg downward control-surface rotation.

Plots of ε against dynamic pressure were generated at various Mach numbers. For the rectangular wing, q ranged from 0 to 350 psf and M varied from 0.7 to 1.5; q ranged from 0 to 80 psi for the fighter model, whereas M varied from 0.7 to 1.10. All analyses were performed retaining a constant sea-level density while matching velocity with dynamic pressure. Pressure coefficients refer to the difference, $C_{p_l} - C_{p_u}$, unless otherwise noted.

Results

Rectangular Wing

Figure 3 plots the rigid rolling moment coefficients against Mach number for analyses using linear ASTROS, linear CAP–TSD, and nonlinear CAP–TSD representations of the steady aerodynamics. This figure indicates that the ASTROS and CAP–TSD linear methods compare well and produce rigid rolling moments that increase with Mach number in the subsonic region and decrease with Mach number at supersonic conditions. The nonlinear CAP–TSD results compare well with the linear CAP–TSD results for Mach numbers up to approximately 0.85 in the subsonic region and then diverge rapidly. The nonlinear method predicts a much larger rigid rolling moment in the region between Mach 0.85 and 0.95. The rigid nonlinear rolling moment then drops off suddenly relative to the linear case.

Figures 4 and 5 show the rigid resultant pressure coefficients for the linear CAP–TSD aerodynamics and the nonlinear CAP–TSD aerodynamics at Mach 0.90. From these figures it can be seen that the deflected control surface produces a considerable increase in resultant pressure on the wing for the nonlinear analysis. This increase in pressure is responsible for the large increase in rigid rolling moment.

Investigation of the effects of structural flexibility began with the determination of control-surface effectiveness ε. Figure 6 shows the ratio of flexible to rigid rolling moment co-

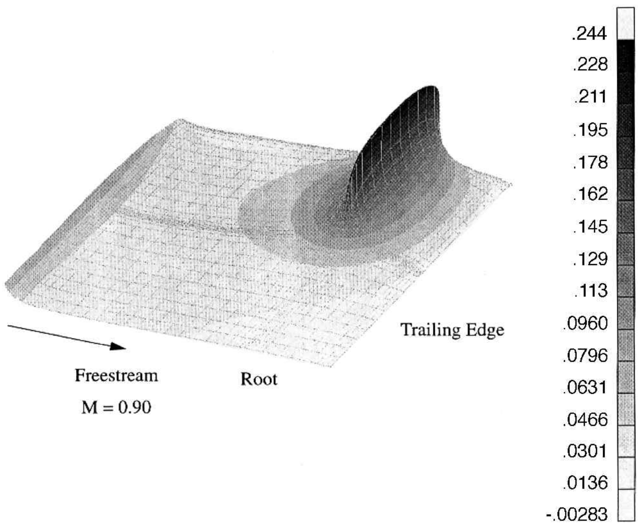

Fig. 4 Rigid linear resultant pressure distribution for rectangular wing.

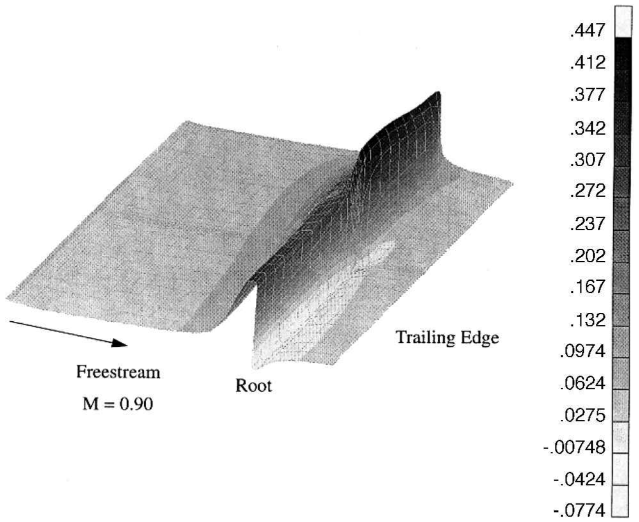

Fig. 5 Rigid nonlinear resultant pressure distribution for rectangular wing.

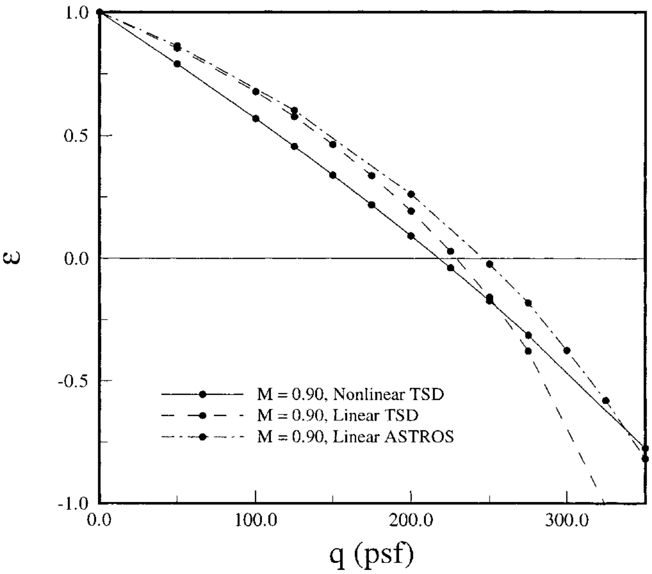

Fig. 6 Variation of control-surface effectiveness with dynamic pressure for rectangular wing.

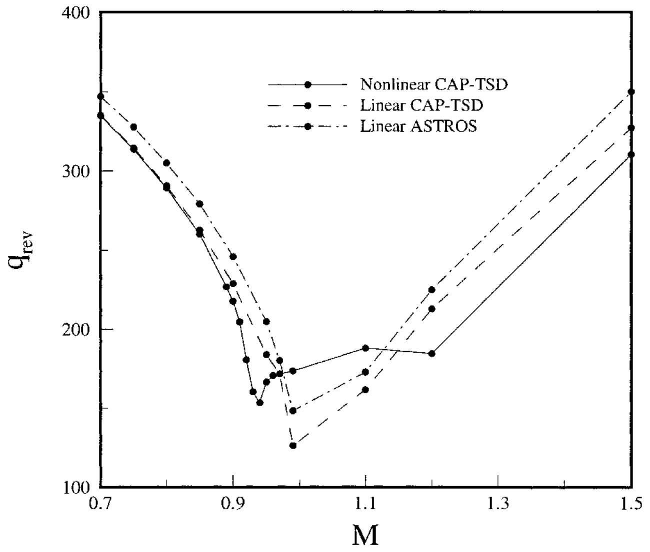

Fig. 7 Control-surface reversal dynamic pressures for rectangular wing.

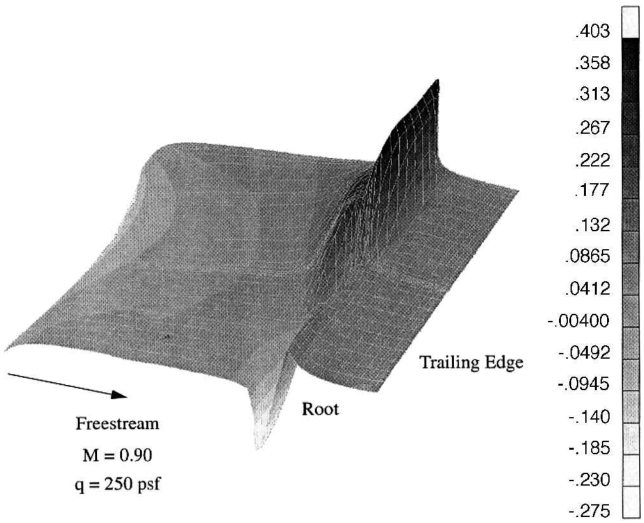

Fig. 8 Aeroelastic nonlinear resultant pressure distribution for rectangular wing.

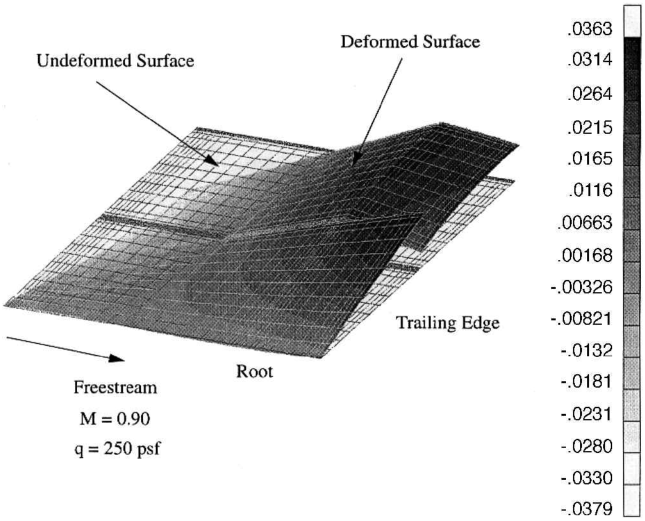

Fig. 9 Aeroelastic deformation of rectangular wing because of control-surface deflection.

efficient at a Mach number of 0.90 with a dynamic pressure ranging from 0.0 to 350.0 psf. Results are again shown for linear ASTROS, linear CAP–TSD, and nonlinear CAP–TSD analyses. An important observation is that the plot of the nonlinear CAP–TSD effectiveness values has less curvature than either of the curves resulting from a linear analysis.

The change in reversal dynamic pressure with respect to Mach number is shown in Fig. 7. This plot indicates that for linear aerodynamics the reversal dynamic pressure decreases with an increase in the Mach number for subsonic conditions and increases with the Mach number in the supersonic regime. The nonlinear results indicate similar trends at subsonic Mach numbers below 0.85 and supersonic Mach numbers above 1.10. At approximately Mach 0.90, however, the nonlinear reversal dynamic pressure decreases rapidly, reaching its lowest value at Mach 0.95, and then begins to increase. This behavior is significantly different than that predicted by the linear analysis.

Some explanation for the drop in reversal dynamic pressure can be found in Fig. 8, which is the resultant pressure distribution for a postreversal aeroelastic analysis at a Mach number of 0.90 and dynamic pressure of 250 psf. From Fig. 8 it can be seen that the downward twisting of the wing produced by the deflected control surface (shown in Fig. 9) has significantly altered the pressure distribution from that of the linear case (Fig. 5). At the wing root, the sign of the pressure rise has changed, resulting in a lower flexible rolling moment.

Fighter Wing

Examination of results for the fighter wing model begins with the chordwise pressure distributions illustrated in Figs. 10 and 11. Four distinct cases are shown in each plot and include pressures for rigid nonlinear, rigid linear, aeroelastic nonlinear, and aeroelastic linear analyses. These pressures are located at 60% of the wingspan. Dynamic pressures for the aeroelastic analyses were chosen to be slightly below the reversal dynamic pressure at the prescribed Mach number. Figure 10 shows pressure distributions at Mach 0.70. The dynamic pressure for the aeroelastic analyses was 60 psi. Figure 11 displays pressures at a transonic flight condition where the Mach number is 0.94. In this case the dynamic pressure for the aeroelastic analyses was 30 psi.

Examination of these pressure distributions obtained from the four analyses reveals the importance of including structural flexibility and flow nonlinearities in the analysis. For flight conditions where the Mach number is low enough to ensure no shocks form on the wing surface, differences between the linear and nonlinear cases are negligible (Fig. 10). At Mach

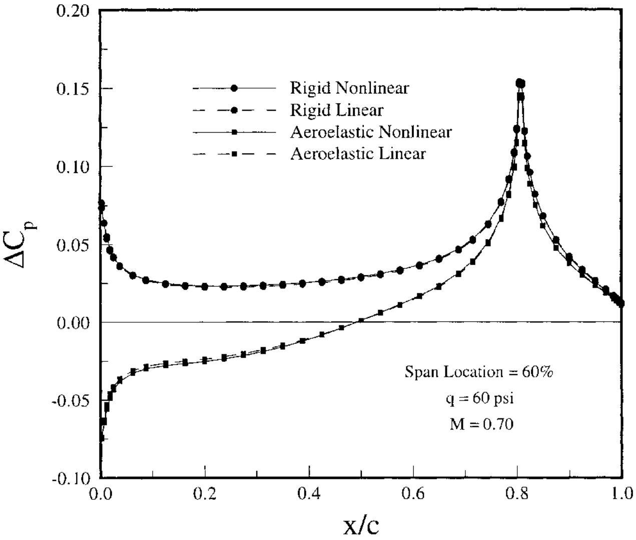

Fig. 10 Chordwise resultant pressure distribution for fighter wing at subsonic conditions.

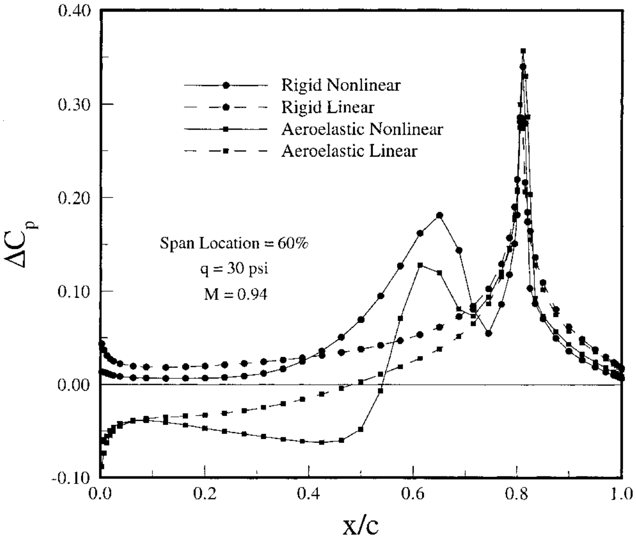

Fig. 11 Chordwise resultant pressure distribution for fighter wing at transonic conditions.

numbers where transonic conditions exist, however, the effects of aerodynamic nonlinearities become pronounced as the pressure distributions in Fig. 11 illustrate. It should be noted that the effects of structural flexibility in the aeroelastic analyses are significant even with the relatively stiff structure used in this model.

A more qualitative examination of the effects of structural flexibility and flow nonlinearities can be observed in Figs. 12–15. These figures depict resultant pressure distributions resulting from a 1-deg downward control-surface deflection for a transonic flight condition at a Mach number of 0.94 and dynamic pressure of 30 psi. Figure 12 shows the pressure distribution for a rigid linear analysis. In this case, the only large chordwise pressure gradient predicted is caused by the control-surface deflection and is located at the control-surface hinge line.

A markedly different pressure distribution is obtained when the effects of transonic aerodynamics are included in the analysis, as illustrated in Fig. 13. In addition to the effects on the pressure distribution caused by the control-surface deflection, the effect of the shocks becomes apparent in the form of a pressure rise near the shocks on the upper and lower surface of the wing.

Figures 14 and 15 show the effects of including structural flexibility in the analysis. Here, negative pressure coefficients are found near the leading edge. As expected, this occurs as the deflected control-surface aeroelastically twists the wing leading edge downward (Fig. 15). Comparison of Figs. 13 and 14 reveals another aeroelastic effect. As increased camber is generated by the deflection of the control surface, the location of the additional pressure spike is shifted upstream, particularly near the root of the wing.

The results presented in the preceding figures indicate the importance of including structural flexibility and flow nonlinearities in the transonic regime. Effects of the shocks, control-surface deflection, and structural flexibility on the pressure dis-

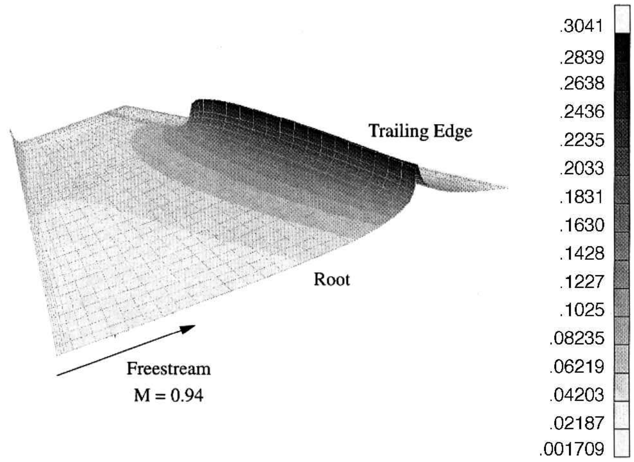

Fig. 12 Rigid linear pressure distribution for fighter wing.

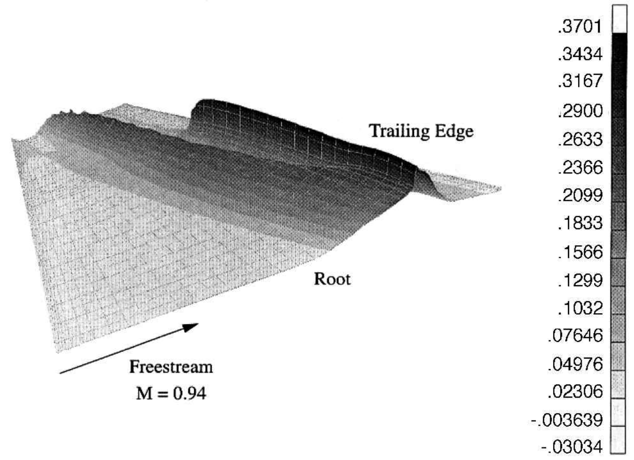

Fig. 13 Rigid nonlinear pressure distribution for fighter wing.

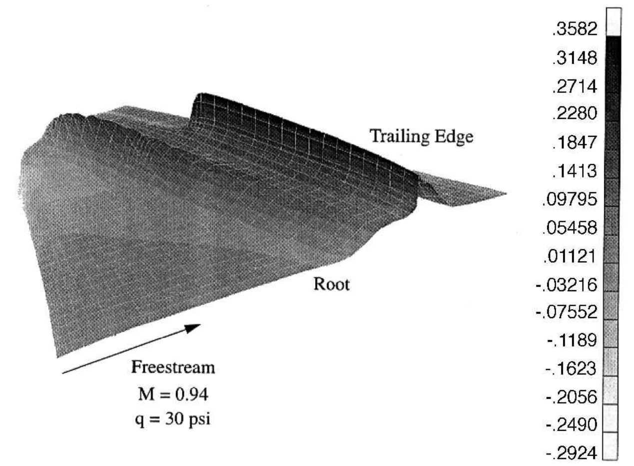

Fig. 14 Aeroelastic nonlinear pressure distribution for fighter wing.

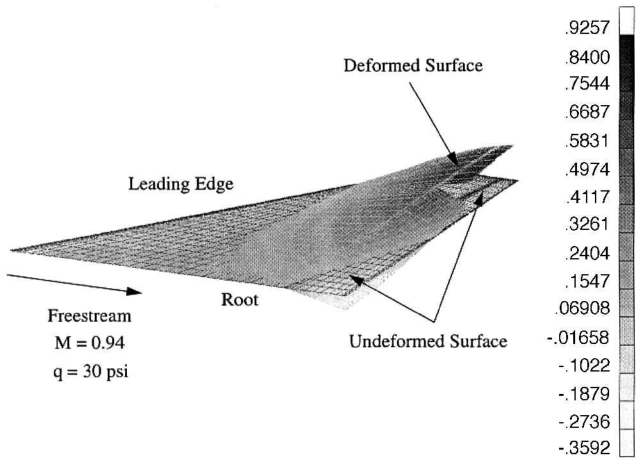

Fig. 15 Aeroelastic deformation of fighter wing because of control-surface deflection.

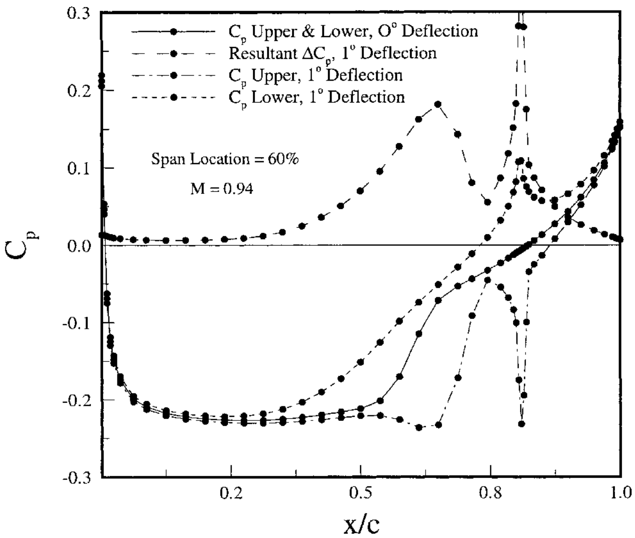

Fig. 16 Chordwise rigid pressure coefficients for fighter wing because of 1-deg downward control surface deflection.

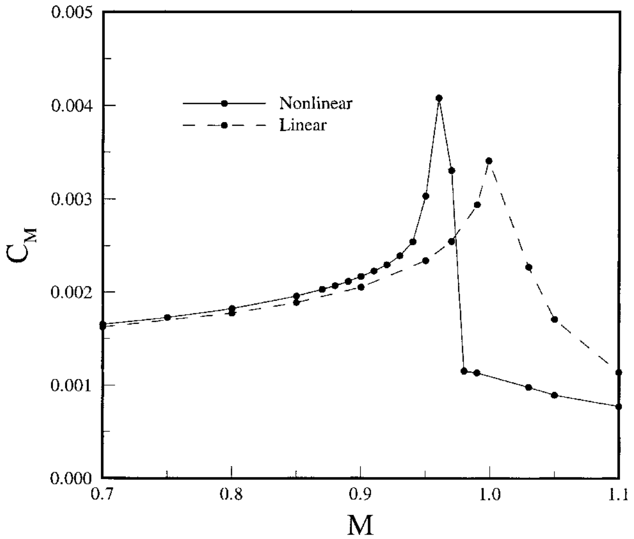

Fig. 17 Variation of rigid rolling moment coefficient with Mach number for fighter wing.

tribution are interdependent and are most accurately obtained through a nonlinear aeroelastic analysis.

The mechanism leading to the pressure rise near the shocks is illustrated in Fig. 16. The chordwise pressure coefficient distribution on the wing with no control-surface deflection is shown for the rigid case (solid line). At this condition a shock forms at approximately 60% of the chord. Because of symmetry, the upper and lower surface pressure distributions are identical. Deflection of the control surface alters this distribution. The lower surface pressure distribution (short dashed line) and the upper surface distribution (dashed and dotted line) are shown for a 1-deg downward control-surface deflection. The deflection of the control surface alters the location and the pressure gradient across the shocks. The higher pressure on the lower surface weakens the shock, allowing the pressure field to propagate farther upstream than on the upper surface. The result (long dashed line) is a region between the upper and lower shocks, where ΔC_p is substantially increased. Because of this effect, it is clear that the locations of the shocks in the presence of control-surface deflections are an important factor in the aeroelastic analysis of wing structures subject to transonic flow conditions.

Because the focus of this research was on rolling maneuver performance in the transonic regime, results measuring this performance were generated. To examine the baseline rolling behavior in the transonic regime, the rolling moment coefficient caused by a 1-deg downward control surface rotation was calculated for the rigid case and is shown in Fig. 17. The significance of including nonlinear aerodynamics are apparent in the Mach number range of 0.92–1.10. Although both linear and nonlinear analyses predict a rise in the rolling moment at high Mach numbers, the effect is magnified by the presence of the shock. Interaction between the shock and control surface is clearly shown beginning with Mach 0.92 and lasting until Mach 0.96. Between Mach 0.96–0.98, the nonlinear rolling moment decreases rapidly. This is most likely caused by the shocks, particularly the shock on the lower surface, nearing and then moving downstream of the control-surface hinge line. When this occurs the shocks no longer constrain the forward propagation of the pressure field as shown in Fig. 16 and the pressure rise between the shocks no longer occurs. As expected, the linear analysis does not capture any of these effects, maintaining a purely subsonic trend up to Mach 1.0 and supersonic behavior beyond.

The influence of structural flexibility is quantified through the control-surface effectiveness value. Figure 18 plots ε against q for Mach numbers of 0.70, 0.94, and 1.05 for both linear and nonlinear analyses. At Mach 0.70, the flow is entirely subsonic and, as expected, the linear and nonlinear results are in close agreement. For the supersonic case, the linear and nonlinear analyses yield similar trends, although the nonlinear predictions are higher. In the transonic region, a significant qualitative difference is noted. While the linear results maintain subsonic characteristics, as indicated by a nearly straight plot, the nonlinear plot more closely resembles the data obtained from the supersonic analyses, particularly at higher dynamic pressures beyond reversal. The nonlinear analysis more completely models the interactions between the shocks and control surface and yields the shown difference between the linear and nonlinear transonic results.

To obtain control-surface reversal points, curves of ε against q were generated for a range of Mach numbers. At each Mach number of interest, the corresponding curve was examined and the dynamic pressure at which the curve crossed zero was noted. The reversal dynamic pressure was interpolated from piecewise linear fits between data points obtained from these analyses. The resulting plot of control-surface reversal dynamic pressures against Mach number is given in Fig. 19 for both the linear and nonlinear aeroelastic analyses. Again, there is a difference between the linear and nonlinear analyses, particularly in the transonic region from approximately Mach 0.90 to Mach 1.10. The nonlinear analysis predicts lower reversal dynamic pressures for subsonic freestream Mach numbers while predicting higher reversal points for supersonic freestream conditions.

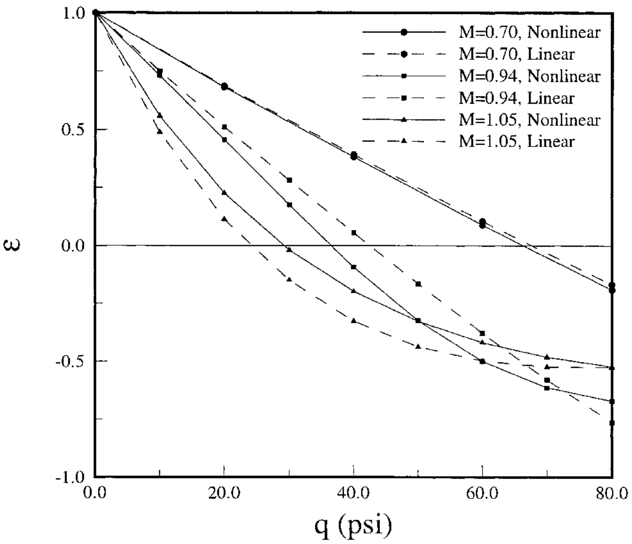

Fig. 18 Variation of control-surface effectiveness with Mach number for fighter wing.

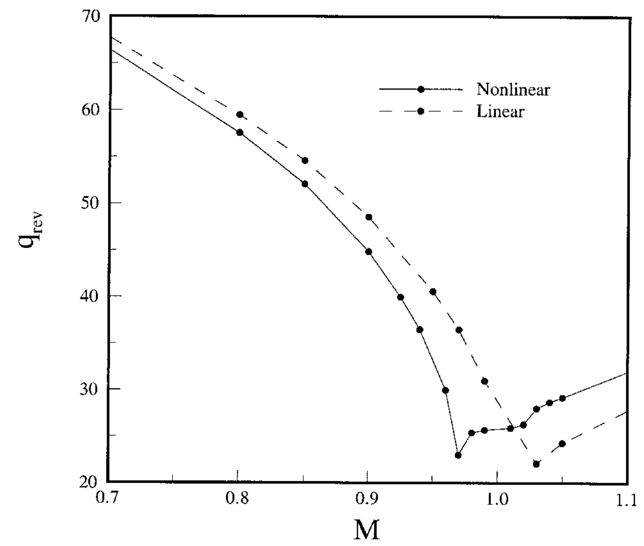

Fig. 19 Variation of control-surface reversal dynamic pressure with Mach number for fighter wing.

The difference between the reversal points for the linear and nonlinear cases in the transonic region is consistent with the differences in the pressure distribution observed between the analyses. In the linear analysis the pressure field produced by the deflection of the control surface twists the wing leading edge downward. This was expected because the large pressure spike at the hinge line is aft of the elastic axis. This aeroelastic deformation produces negative pressures at the leading edge of the wing, resulting in reduced roll effectiveness.

This effect is magnified when the aerodynamic nonlinearities caused by the shock are included. As the pressure spike between the shocks moves aft of the elastic axis, there is an additional contribution to the twisting of the wing. This effect builds until the shocks move behind the control-surface hinge line, in this case at approximately Mach 0.97. Beyond this Mach number the reversal point rises again and begins to approach the linear supersonic results.

Qualitatively, the trends seen in control-surface reversal points in Fig. 19 are similar to those seen for the rigid rolling moments in Fig. 17, and once again indicate the importance of including flow nonlinearities in aeroelastic analyses in the transonic regime. Effects of the control-surface deflection are magnified by the presence of shock waves located upstream of the control-surface hinge line. In the rigid case, this effect serves to augment the roll effectiveness of the control surface. When flexibility effects are included, however, the effect of the shocks constraining the pressure field increases the adverse twisting of the wing, resulting in decreased roll effectiveness and lower reversal speeds.

Conclusions

The aeroelastic analyses of the wing models demonstrates that the presence of shocks on the surface of the wing has a significant impact on the steady aeroelastic characteristics of the wing. Although trends appear to be somewhat dependent on the physical configuration of the model, predictions of rolling moment coefficients, control-surface effectiveness values, and reversal dynamic pressures differ considerably in the transonic regime, depending on whether linear or nonlinear analyses are performed.

Examination of pressure distributions indicates that the presence of shocks forward of the control-surface hinge line constrains the forward propagation of the pressure field produced by a control-surface deflection. This in turn causes a pressure difference in the region of the shocks that alters the effect of the control deflection. This generally augments the rigid rolling moment but increases adverse twist over that predicted by a linear analysis when structural flexibility is included. Consequently, this degrades control-surface effectiveness values and lowers the reversal dynamic pressure in the transonic region.

Finally, it should be noted that the accuracy of the results presented in this paper are not absolute. Comparison of results to higher-order computational fluid dynamics codes was not undertaken. Furthermore, lack of experimental or flight test data for purposes of comparison makes substantiation of the reported data difficult. The use of Navier–Stokes computational fluid dynamics may show that viscous effects at chordwise and spanwise control surface discontinuities as well as the trailing-edge limit the use of TSD theory to regions where the flow is free of significant viscous effects. For these reasons, care should be taken when considering the results of this study as quantitative. Until further data substantiation is completed, the qualitative trends revealed in this investigation may be the most useful results.

References

[1]Sotamayer, W. A., "Unsteady Transonic Flow for a Wing with Control Surface Deflections," U.S. Air Force Wright Aeronautical Lab., TM-86-186-FIBR, Wright–Patterson AFB, OH, Jan. 1987.

[2]Bharadvaj, B. K., "Computation of Steady and Unsteady Control Surface Loads in Transonic Flow," *AIAA/ASME/ASCE/AHS/ASC 31st Structures, Structural Dynamics, and Materials Conference* (Long Beach, CA), AIAA, Washington, DC, 1990, pp. 1349–1360.

[3]Pitt, D. M., and Fuglsang, D. F., "Aeroelastic Calculations for Fighter Aircraft Using the Transonic Small Disturbance Equation," *AGARD Conference Proceedings 507 Transonic Unsteady Aerodynamics and Aeroelasticity*, AGARD, Neuilly Sur Seine, France, 1992, pp. 16-1–16-11.

[4]Miller, G. D., "Active Flexible Wing (AFW) Technology," U.S. Air Force Wright Aeronautical Lab., TR-87-3096, Wright–Patterson AFB, OH, Feb. 1988.

[5]Batina, J. T., "A Finite-Difference Approximate-Factorization Algorithm for Solution of the Unsteady Transonic Small-Disturbance Equation," NASA TP 3129, Jan. 1992.

[6]Johnson, E. H., and Venkayya, V. B., "Automated Structural Optimization System (ASTROS)," *Theoretical Manual*, Vol. 1, U.S. Air Force Wright Aeronautical Lab., TR-88-3028, Wright–Patterson AFB, OH, Dec. 1988.

[7]Harter, R. L., and Desmarais, R. N., "Interpolation Using Surface Splines," *Journal of Aircraft*, Vol. 9, No. 2, 1972, pp. 189–191.

[8]Canfield, R. A., and Jacques, D., "Effect of Modal Sensitivity on Flutter Eigenvalue Derivatives," *AIAA/ASME/ASCE/AHS/ASC 35th Structures, Structural Dynamics, and Materials Conference* (Hilton Head, SC), AIAA, Washington, DC, 1994, pp. 1764–1770.

[9]Stritz, A. G., Eastep, F. E., and Venkayya, V. B., "Influence of Static and Dynamic Aeroelastic Constraints on the Optimal Structural Design of Flight Vehicle Structures," *Proceedings of the AIAA/ASME/ASCE/AHS/ASC 32nd Structures, Structural Dynamics, and Materials Conference* (Baltimore, MD), AIAA, Washington, DC, 1991, pp. 470–476.